Modulation of Thermospheric Circulation by Lower-Thermospheric Winter-to-Summer Circulation: The Atmosphere Gear Effect

Jack C. Wang[1,2], Jia Yue[1,2], Wenbin Wang[3], Liying Qian[3]

[1]Catholic University of America, Washington, DC, USA
[2]NASA Goddard Space Flight Center, Greenbelt, MD, USA
[3]High Altitude Observatory, National Center for Atmospheric Research, Boulder, CO, USA

Key Points:

- The lower-thermospheric circulation enhances the circulation in the summer thermosphere and strengthens upwelling in higher latitudes.
- Including the lower-thermospheric circulation in the model improves agreement with observed semi-annual oscillation in mass density.
- This study reveals a new coupling pathway, “atmospheric gear effect”, linking the lower and upper atmosphere.

Corresponding author: Jack C. Wang, `jack.c.wang@nasa.gov`

Abstract

This study investigates the impact of the lower-thermospheric winter-to-summer circulation on the thermosphere's thermal structure and meridional circulation. Using NCAR TIE-GCM, we compare simulations with and without the lower-thermospheric circulation, finding that its inclusion enhances summer-to-winter thermospheric circulation by 40% in the summer hemisphere but decelerates it in the winter thermosphere. Meanwhile, vertical wind exhibits stronger upward motion poleward of $\pm 30°$ latitude above 10^{-6} hPa ($\sim$174 km) when lower-thermospheric circulation is incorporated. This dynamic coupling functions as an atmospheric "gear mechanism", accelerating momentum and energy transfer to higher altitudes. Including lower-thermospheric circulation improves agreement between the nudged run and NRLMSIS 2.1 in intra-annual variability (IAV) of mass density. This suggests lower-thermospheric circulation is a key factor in modulating IAV in the coupled thermosphere-ionosphere system. This study reveals a new coupling mechanism between the lower atmosphere, thermosphere, and ionosphere, with significant implications for understanding upper-atmospheric dynamics and improving space weather models.

Plain Language Summary

We explore how meridional circulation in the lower thermosphere affects the coupled thermosphere-ionosphere system. A narrow lower-thermospheric winter-to-summer circulation, driven by tides and gravity waves from lower atmosphere, is absent in models with a lower boundary above the mesopause. Through a numerical sensitivity experiment, we found that incorporating lower-thermospheric circulation into TIE-GCM via nudging (or Newtonian relaxation) strengthens summer thermospheric circulation by about 40% but decelerates it in the winter hemisphere. To maintain mass continuity, additional upwelling occurs poleward of $\pm 30°$ latitude above 10^{-6} hPa ($\sim$174 km) when lower-thermospheric circulation is included. This interaction acts as a "gear mechanism", facilitating energy and momentum transfer across atmospheric layers. We also found that lower-thermospheric circulation influences intra-annual variations in thermospheric mass density, improving agreement with the empirical model NRLMSIS 2.1. This study highlights the key connection between the lower and upper atmosphere, revealing a new coupling pathway. Our findings have practical implications for atmospheric and space weather research, particularly in improving thermospheric density modeling, which is crucial for satellite operations, mitigating drag-related risks, and supporting collision avoidance. Moreover, it underscores the importance of accurately representing lower-atmospheric dynamics in upper-atmosphere models to advance predictive modeling of thermosphere-ionosphere interactions.

1 Introduction

The mesosphere and lower thermosphere (MLT) span approximately 50–110 km altitude. Within the MLT, wave forcing from gravity waves (GWs) in the mesosphere, as well as tides and GWs in the lower thermosphere along with Coriolis force drive meridional circulations (Holton & Alexander, 2000; J. C. Wang et al., 2022). The meridional circulations are mainly pole-to-pole during solstices. In the mesosphere, the meridional wind flows from the summer to the winter hemisphere, but the flow reverses to winter-to-summer in the lower thermosphere. This winter-to-summer lower-thermospheric circulation is a consequence of a balance between the Coriolis force and the zonal momentum forcing associated with dissipation of tides and inertia gravity waves (GWs) (e.g., J. C. Wang et al., 2022). Note that mesoscale GWs with the zonal wavenumber larger than 30 cannot be fully resolved in the model simulations in J. C. Wang et al. (2022), because these waves are too small to be resolved and therefore strongly dissipated by numerical diffusion. This deficiency may lead to a weaker meridional circulation in the model simulation compared to the observations. The lower-thermospheric circulation is virtually absent in models where the lower boundary is located above the mesopause (e.g., Qian & Yue, 2017; Malhotra et al., 2022; Forbes et al., 2024).

Above the lower-thermospheric circulation, the meridional circulation reverses direction once again, flowing from summer to winter in the middle-to-upper thermosphere (hereafter referred to as the thermospheric circulation, ranging from ∼150 km to 500 km). This thermospheric circulation is primarily driven by the pressure gradient force, which results from the hemispheric asymmetry in solar heating due to the obliquity of the celestial body (Dickinson et al., 1977; Roble et al., 1987). The pressure gradient force, which varies both spatially and temporally, is mainly balanced by ion drag, the Coriolis force, and viscosity (Hsu et al., 2016).

Vertical advection by the lower-thermospheric circulation modulates the atomic oxygen (O) budget around the base of the thermosphere and causes a hemispheric asymmetry of O profile during the solstices (J. C. Wang et al., 2023). Vertical transport process of O in the MLT has a crucial impact on the coupled ionosphere and thermosphere system (e.g., Yamazaki & Richmond, 2013; Siskind et al., 2014; Qian & Yue, 2017). Once the abundance of O is modulated at lower altitudes, its net effect can propagate into higher altitudes and alter the electron and neutral densities in the coupled system of the ionosphere and thermosphere (Bates, 1959; Yamazaki & Richmond, 2013; Qian & Yue, 2017).

In the mesosphere, to maintain mass continuity, vertical wind must adjust to balance changes in the meridional wind. The adjustments in vertical wind lead to changes in the meridional temperature gradient and the vertical gradient of zonally-averaged zonal wind, ensuring that the thermal wind balance remains valid in the presence of wave forcing and diabatic heating (Holton & Hakim, 2013). This dynamical adjustment results in temperatures at the winter mesopause being warmer than radiative equilibrium and cooler at the summer mesopause due to adiabatic heating and cooling, respectively. These processes also contribute to the observed hemispheric asymmetry in mesopause height, as reported by SABER observations (Xu et al., 2007; N. Wang et al., 2022). Similar to the mesospheric circulation, recent model simulations demonstrate that the changes in the vertical wind associated with the thermospheric circulation produce additional adiabatic heating/cooling and modify the thermospheric thermal structure (Forbes et al., 2024). Likewise, adiabatic heating and cooling via vertical displacement, associated with the lower-thermospheric circulation, should be able to modulate the thermal structure. However, the impact of this adiabatic heating and cooling is challenging to observe and distinguish from diabatic heating, such as Joule heating and heat conduction, due to the sparse coverage of profiles in both local time and spatial distribution available to probe this region of the atmosphere (Mlynczak et al., 2021). Recent work has addressed this challenge by quantifying adiabatic cooling and warming in the mesosphere and lower thermosphere using SABER CO_2 VMR vertical displacements, revealing a distinct yet previously overlooked layer of adiabatic warming (cooling) in the summer (winter) lower thermosphere (Yue & Wang, 2025).

The primary objective of this study is to investigate how the lower-thermospheric winter-to-summer circulation influences the thermal structure of the thermosphere and, consequently, the thermospheric circulation. Our results indicate that, when the lower-thermospheric circulation is incorporated into the model (nudged run), the thermospheric circulation above is enhanced by 40% in the summer hemisphere but decelerated in the winter thermosphere compared to the base run without lower thermospheric circulation. Incorporating the lower-thermospheric circulation in the model simulation induces additional upwelling in the higher latitudes of the thermosphere, which, in turn, improves the intra-annual variation (IAV) in thermospheric mass density in the nudged run. This result indicates that the lower-thermospheric circulation may play a key role in modulating both the amplitude and phase of the IAV in thermospheric mass density. This study proposes a new coupling mechanism between the lower and upper thermosphere, based on first-principles modeling. Because the lower thermosphere is controlled by waves from below, this study demonstrates a new lower atmosphere-thermosphere-ionosphere coupling pathway.

2 Modeling approach

The NCAR TIE-GCM is a three-dimensional model that represents the coupled thermosphere and ionosphere system, incorporating self-consistent electrodynamics. It solves three-dimensional equations governing ion and neutral momentum, energy, and continuity on constant pressure levels. In this study, version 3.0 of the TIE-GCM is utilized. The spatial grid resolution is 2.5° in both latitude and longitude, with a vertical resolution of one-quarter scale height. The model's lower boundary is located around 97 km altitude (at $z = z_{\text{bot}} = -7$, where $z = \ln \frac{p_0}{p}$ and $p_0 = 5 \times 10^{-7}$ hPa). The current version of TIE-GCM offers three configurations for the upper boundary. For this study, the upper boundary is set at $z = 9$, which corresponds to approximately 700 km altitude under solar minimum conditions.

The lower-thermospheric circulation is driven by resolved wave forcing, including tides and inertia GWs from the lower atmosphere (J. C. Wang et al., 2022). The lower-thermospheric circulation cannot be internally generated in the TIE-GCM, as migrating and non-migrating tidal perturbations are specified at the lower boundary (∼97 km) by the Global Scale Wave Model (GSWM; Hagan & Forbes, 2002, 2003). This configuration is referred to as the *base run* throughout the remainder of the manuscript.

To assess the impact of the lower-thermospheric circulation on the thermosphere, a sensitivity experiment is performed using the nudging technique (Siskind & Drob, 2014; Maute et al., 2015; J. C. Wang et al., 2017; Jones, Drob, et al., 2018), referred to as the *nudged run*. Nudging could help compensate for missing physics (e.g., GW forcing) compared to a fully self-consistent model (Ren et al., 2011; Siskind & Drob, 2014). In the nudged run, horizontal winds, temperature, and geopotential height (Z) are constrained at every model time step between the lower boundary ($z_{\text{bot}} = -7$) and $z = -3$ ($p \approx 10^{-5}$ hPa or $\sim$128 km) using 3-hour output from 2009 simulations in the Specified Dynamics configuration of the Whole Atmosphere Community Climate Model eXtended (SD-WACCMX) version 6.2 (J. Liu et al., 2018; H.-L. Liu et al., 2018). The meridional wind from SD-WACCMX, validated against TIMED Doppler Interferometer (TIDI) observations, shows qualitative agreement but is $\sim$50% weaker partially due to underestimated sub-grid GW forcing (J. C. Wang et al., 2022). Consequently, the modulation of thermospheric circulation by the lower-thermospheric circulation in this study represents a lower limit, as stronger wave forcing would enhance the lower-thermospheric circulation and its impact on the thermospheric circulation.

However, some limitations remain. First, only one-way upward coupling is considered, but this does not affect our findings since the focus is on how lower-thermospheric circulation modulates thermospheric circulation. Second, discontinuities may occur at the model interface (e.g., Siskind & Drob, 2014; J. C. Wang et al., 2017; Jones, Drob, et al., 2018), which we mitigate using a vertical weighting function, $\zeta(z) = \exp\left(-(z - z_{bot})/0.8\right)$, ensuring a smooth transition. Above $z = -3$, the model is essentially free-running. A similar approach was used by Siskind and Drob (2014). Results from the nudged and base runs will be compared to quantify the impact of the lower-thermospheric circulation on the thermosphere.

Each model run is executed over the course of one year under solar minimum conditions, with a same upper boundary condition: $F_{10.7} = 70$, crosstail potential = 30 kV, and hemispheric power = 18 GW. The eddy-diffusion coefficient (K_{zz}) in both runs is time- and location-invariant. When comparing the tidal structure and the divergence of momentum flux between the nudged and base runs, we found that the difference in the momentum budget due to tidal dissipation is negligible over seasonal timescales. The change in meridional circulation between the nudged and base runs is primarily due to differences in the background atmosphere, as will be demonstrated in the following section.

3 Results

Figures 1a to d show the diurnally and zonally averaged meridional wind ($\overline{\mathrm{V}}$) in the thermosphere during the June solstice of the year 2009 from the base and nudged runs. A similar but opposite feature of $\overline{\mathrm{V}}$ during the December solstice is illustrated in Figure S1 in the supplement. The solstices are selected for this analysis because the thermospheric circulation is significantly stronger during solstices compared to equinoxes. During the equinoxes, both lower and upper thermospheric circulations transition between the summer and winter state, resulting in a relatively weaker magnitude of large-scale $\overline{\mathrm{V}}$ throughout the thermosphere (Gan et al., 2024). The meridional wind predominantly moves from the summer to the winter hemisphere above $2{\times}10^{-5}$ hPa (∼119 km) (Figures 1a and b). This summer-to-winter thermospheric circulation is primarily driven by the pressure gradient force resulting from the seasonal difference in solar radiation. The magnitude of $\overline{\mathrm{V}}$ can reach around 40 m/s in the upper thermosphere.

$\overline{\mathrm{V}}$ in the lower thermosphere is considerably weaker than at higher altitudes; therefore, it is plotted on different contour scales in Figures 1c and 1d. In the base run, the lower-thermospheric circulation is virtually absent (Figure 1c). Instead, a cell-like structure with poleward flow on both sides of the equator appears around 10^{-4} hPa, mainly induced by the dissipation of the migrating diurnal tide (Yamazaki & Richmond, 2013). In the nudged run, the magnitude of the winter-to-summer meridional wind reaches up to 6 m/s between $6{\times}10^{-5}$ and $2{\times}10^{-5}$ hPa (Figure 1d).

When the lower-thermospheric winter-to-summer circulation is imposed in the model, the summer-to-winter thermospheric circulation strengthens by up to 12 m/s or 40% between 10^{-5} and 10^{-6} hPa (roughly between 128 km to ∼174 km) and 30°S to 15°N latitude, as shown in Figure 1e. The increase in meridional wind extends up to 10^{-9} hPa (∼415 km) in the summer hemisphere, likely because the imposed lower-thermospheric circulation has a larger magnitude in the summer hemisphere. However, an additional clockwise circulation is induced in the winter thermosphere, opposing the summer-to-winter circulation, between 50°S and 10°S latitude above 10^{-7} hPa (∼239 km).

Figure 1f illustrates the change in mean vertical wind ($\Delta\overline{\mathrm{W}}$) between the nudged and base runs. A notable feature is the enhanced upward motion poleward of ±30° latitude above ∼10^{-7} hPa (239 km) during the solstices (Figures 1f and S1f). This induced

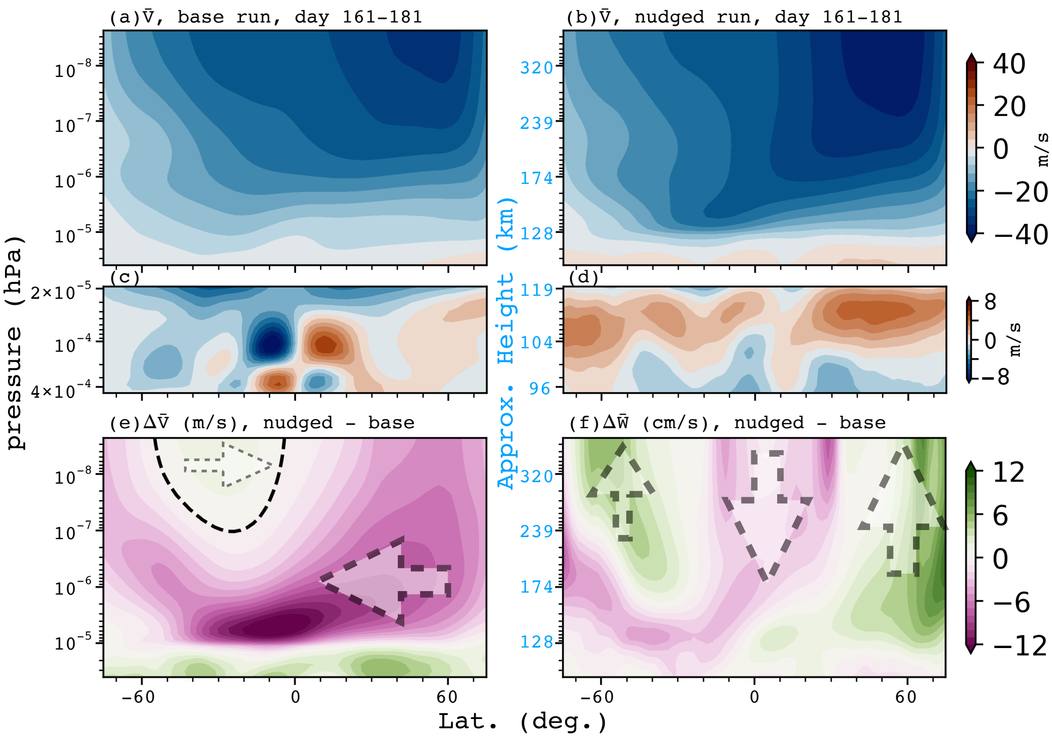

Figure 1. (a-d) $\overline{\mathrm{V}}$ as a function of pressure level and latitude from (a and c) the base run, (b and d) the nudged run on the June Solstice. Contour level is 4 m/s in Figures 1a and 1b, and 1 m/s in Figures 1c and 1d. Positive is northward. (e-f) The differences in (e) $\overline{\mathrm{V}}$ and (f) $\overline{\mathrm{W}}$ between the nudged run and the base run. The contour interval is 1 m/s in Figure 1e and 1 cm/s in Figure 1f. Arrows in Figures 1e and 1f indicate the direction of change in meridional and vertical wind. The dashed line in Figure 1e indicates where the difference equals zero. The analysis is averaged over days 161 to 181 of the year 2009. $\overline{\mathrm{V}}$ and $\overline{\mathrm{W}}$ represent the diurnally and zonally averaged meridional and vertical winds, respectively.

upwelling influences seasonal variation and latitudinal distribution of composition. This topic will be further explored in Section 4.

The magnitude and direction of $\overline{\mathrm{V}}$ in the thermosphere are primarily regulated by the pressure gradient force, Coriolis force, ion and viscous drag, and wave forcing. When viscous drag and wave forcing are negligible in the lower atmosphere, the horizontal wind ultimately reaches geostrophic balance. In this balanced state, the geostrophic wind is purely zonal for diurnally and zonally averaged flow by definition (Andrews & McIntyre, 1976). However, geostrophic balance is not achieved in the stratosphere or higher altitudes, where wave forcing, molecular viscosity, and/or ion drag, are strong enough to al-low a mean meridional circulation (Dickinson et al., 1975, 1977; Hsu et al., 2016). In this section, a term analysis is performed to identify the dominant forces driving changes in the thermospheric meridional wind when lower-thermospheric circulation is introduced into the model. Figure 2a shows $\overline{\mathrm{V}}$ averaged over $\pm 60°$ latitude at 2.54×10^{-6} hPa ($\sim$153 km) from the base and nudged runs, with the corresponding pressure gradient force in Figure 2b and the combined Coriolis and ion drag forces in Figure 2c. Individual term of Coriolis and ion drag forces is illustrated in Figure S2 in the supplement. The increase in the pressure gradient force in the nudged run clearly alters $\overline{\mathrm{V}}$, while the Coriolis and ion drag forces adjust in magnitude to balance this change. Hsu et al. (2016) demonstrated that ion drag and viscosity can sufficiently cause the horizontal wind to rotate toward the pressure gradient force.

Geopotential is the vertical integral of neutral temperature, meaning that changes in the thermal structure modify the geopotential at the same level or higher, ultimately leading to adjustments in $\overline{\mathrm{V}}$. An analysis of the mean temperature structure is conducted to illustrate how the thermal structure, influenced by adiabatic heating and cooling from vertical wind changes due to lower-thermospheric circulation, impacts the meridional momentum budget.

The acceleration by the pressure gradient force in $\overline{\mathrm{V}}$ is determined by $\frac{g}{a}\frac{\partial Z}{\partial \phi}$, where Z denotes the geopotential height, a and ϕ are the radius and latitude of the Earth. g is the acceleration of gravity at the lower boundary of the model. In the TIE-GCM, the geopotential height is calculated from the hydrostatic equation by integrating the scale height (H) vertically from the model lower boundary to the given pressure level,

$$Z(z) = \int_{z_{\mathrm{bot}}}^{z} H dz = \int_{z_{\mathrm{bot}}}^{z} \frac{R^* T_n}{\overline{m} g} dz \tag{1}$$

where z is the pressure interface, $z = \ln{(p_0/p)}$. The reference pressure p_0=5×10^{-7} hPa, and p represents isobaric surface. z_{bot} is the model lower boundary, where z_{bot} is equal to -7. R^* is the specific gas constant. T_n is the neutral temperature. $\overline{m}$ denotes the mean molecular weight.

Figure 3a shows the difference in geopotential height between 60°N and 60°S, serving as a proxy for the latitudinal gradient of geopotential height. Below 6.5×10^{-5} hPa, the geopotential height is higher in the Southern hemisphere in the nudged run, a fea-

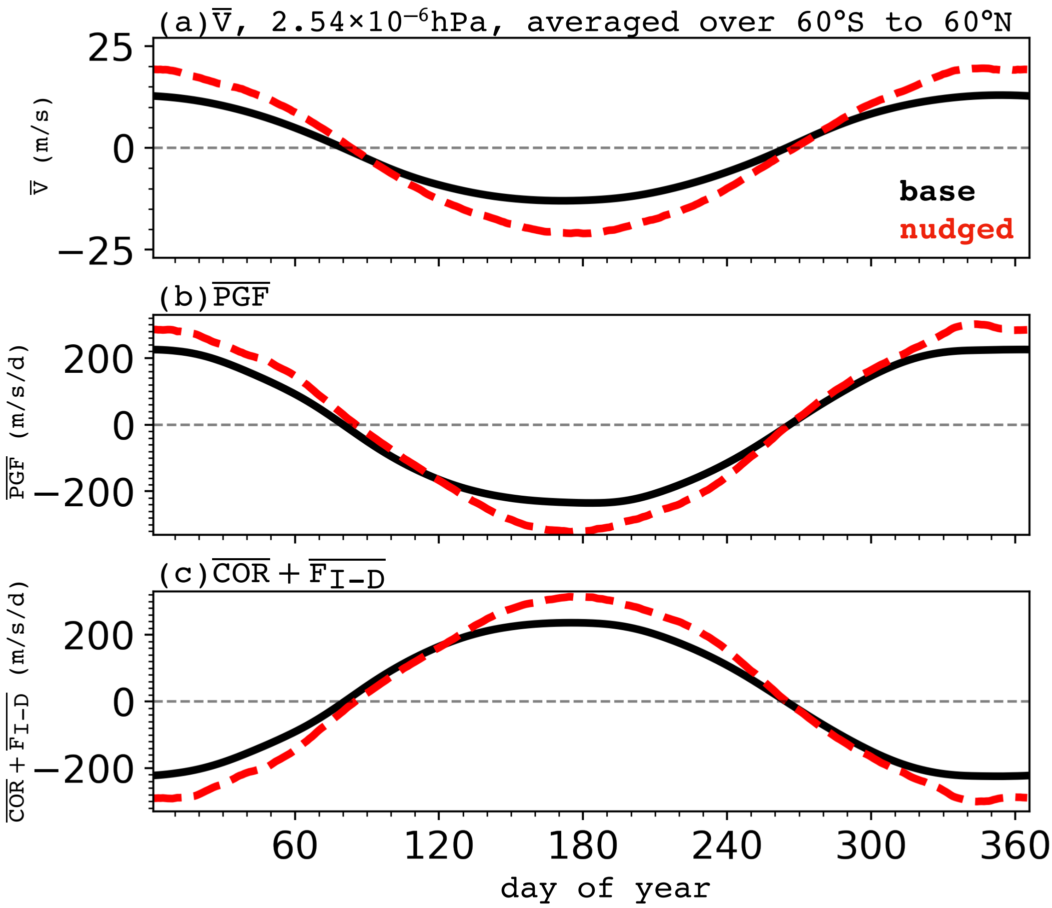

Figure 2. (a) $\overline{V}$ at 2.54×10^{-6} hPa (∼153 km) from (red dashed line) the nudged run and (black line) the base run. Positive is northward. (b) Diurnally- and zonally-averaged pressure gradient force in the meridional direction at 2.54×10^{-6} hPa in a unit of m/s/day. (c) Similar to (b) but for the sum of the diurnally- and zonally-averaged Coriolis force and ion drag force in the meridional direction.

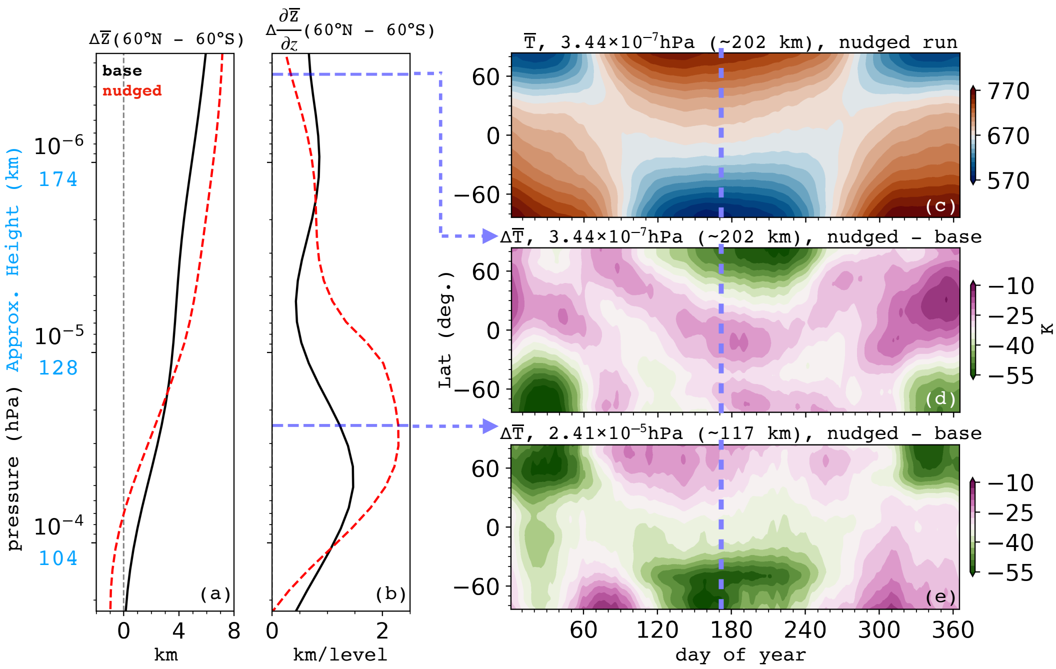

Figure 3. (a) Profile of the difference in the diurnally- and zonally-averaged geopotential height between 60°N and 60°S from (red dashed line) the nudged run and (black line) the base run. (b) Similar to (a) but for vertical gradient difference between 60°N and 60°S. The analysis is averaged between 2009 day 161 to 181, centered at day 171 indicated as the blue dashed line in Figures (c)-(e). (c) Diurnally- and zonally-averaged neutral temperature at 3.44×10^{-7} hPa (∼202 km) from the nudged run. (d) Similar to (c) but for the difference between the nudged and base run. (e) Similar to (d) but for the difference at 2.41×10^{-5} hPa (∼117 km).

ture absent in the base run. This reversal of the summer-to-winter geopotential difference is linked to the temperature structure between the model's lower boundary and 6.5×10^{-5} hPa. In the base run, the temperature and geopotential height at the lower boundary ($z = -7$) are specified by migrating and non-migrating tides from the GSWM, with a constant background temperature of 181 K and a geopotential height of 96.37229 km. In contrast, the nudged run shows a sharp decrease in geopotential height and temperature in the Northern hemisphere at the lower boundary (figure not shown), associated with the cold summer mesopause, a well-known feature in the middle atmosphere (Holton, 1983; Garcia, 1989).

Figure 3b shows the difference in the vertical gradient of geopotential height between 60°N and 60°S. The latitudinal gradient of geopotential height increases more rapidly with altitude in the nudged run due to a stronger latitudinal temperature gradient toward the summer hemisphere between 10^{-4} and 2×10^{-6} hPa (see Equation 1 and Figure 3e). Consequently, the summer-to-winter geopotential height difference is greater in the nudged run compared to the base run above 1.8×10^{-5} hPa. This trend affects scale height and geopotential height, creating a stronger pressure gradient force directed toward the winter hemisphere.

The latitudinal temperature gradient below the lower-thermospheric circulation points more strongly toward the summer hemisphere in the nudged run. However, above the lower-thermospheric circulation, it reverses toward the winter pole (Figures 3d and e). This suggests that changes in vertical wind in the nudged run, as shown in Figure 1f, lead to additional adiabatic heating and cooling, modifying the temperature structure. The global-average neutral temperature in the nudged run is about 20 K cooler than in the base run, but this difference does not affect the simulated meridional wind, as it is the horizontal gradient of temperature, rather than the absolute value, that drives wind changes (Andrews et al., 1987).

4 Impact on thermospheric mass density

As examined earlier, the induced $\Delta\overline{\mathrm{W}}$ associated with the lower-thermospheric circulation is generally upwelling in both hemispheres of the upper thermosphere during solstices (Figure 1f and S1f). The changes in $\Delta\overline{\mathrm{W}}$ impacts the seasonal variation of the composition and its latitudinal distribution. Figures 4a and b show, when the lower-thermospheric

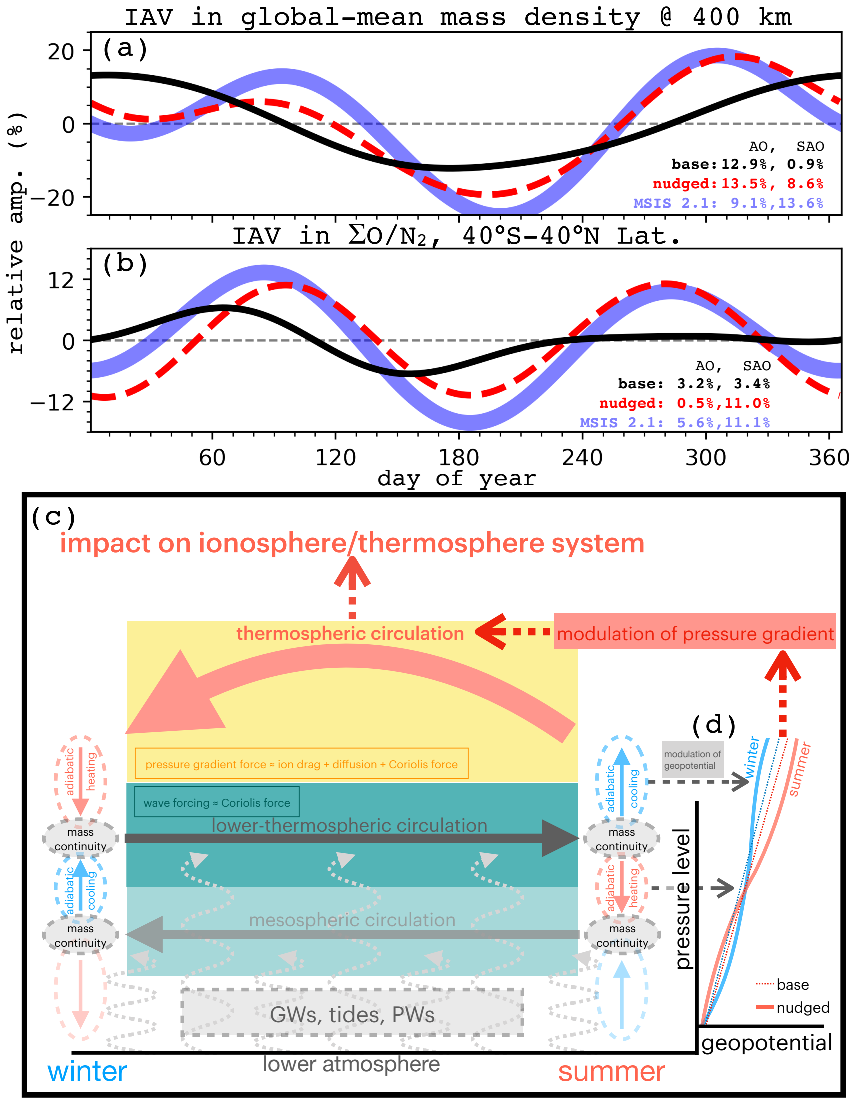

Figure 4. Intra-annual variation (IAV) in (a) globally-averaged mass density at 400 km altitude, (b) Column-integrated O/N$_2$ ratio ($\Sigma O/N_2$) averaged between ±40° latitude, showing percentage changes relative to the annual average. (black solid) the base run, (red dashed) the nudged run, and (blue) NRLMSIS 2.1. The amplitudes of annual and semi-annual variations (AO and SAO) for each run are provided in the bottom right corner of the figure. (c) Schematic of a latitude-pressure cross-section showing the coupling between winter-to-summer lower-thermospheric and summer-to-winter thermospheric circulations. Solid arrows indicate net meridional air motion, while a dashed arrow represents modulating processes. Red and blue dashed circles mark regions of adiabatic heating (downwelling) and cooling (upwelling) linked to meridional mass continuity. Wavy arrows depict upward-propagating gravity waves, tides, and planetary waves, with their dissipation driving mesospheric and lower-thermospheric circulations in the cyan and dark cyan-shaded regions, respectively, indicating opposing wave forcing directions in the mesosphere and lower thermosphere. (d) Schematic of geopotential height as a function of pressure level, with red denoting the summer hemisphere and blue representing the winter hemisphere from (solid) the nudged run and (dashed) base run.

circulation is nudged in the TIE-GCM, a better agreement for the simulated semi-annual oscillation (SAO) in mass density and column-integrated O/N_2 ratio ($\Sigma O/N_2$) can be achieved compared to that in the base run. The amplitude of the SAO in the global-averaged mass density at 400 km is about 8.6% in the nudged run, showing a better agreement with the result in the NRLMSIS 2.1 (US Naval Research Laboratory Mass Spectrometer Incoherent Scatter radar, Emmert et al., 2021, 2022), where the relative amplitude is about 13.6% in the MSIS 2.1. On the other hand, the SAO is virtually absent in the base run (0.9%). The annual variation can reach 13.5% in the nudged run, where the amplitude of the annual oscillation (AO) is about 9.1% in magnitude in the MSIS 2.1.

The IAV in $\Sigma O/N_2$ (Figure 4b) is analyzed over $\pm 40°$ latitude for comparison with satellite observations (Strickland et al., 2004; Qian et al., 2009; Yue et al., 2019; Gan et al., 2023, 2024). In the base run, seasonal variation is weak, particularly in the second half of the year. The nudged run resolves the SAO well, with two similar minima around the solstices, closely aligned with MSIS 2.1. However, the AO is nearly absent, while MSIS 2.1 shows a deeper June solstice minimum. Satellite observations also indicate that AO as a key feature of "global-mean" $\Sigma O/N_2$ (Qian et al., 2009; Yue et al., 2019). Note that "global-mean" here refers to the globally averaged values over the available local times and maximum latitude covered by the field of view of the given instrument. The spatial and temporal coverage of the observations is not uniformly distributed, which may introduce aliasing effects. These results in Figures 4a and b suggest that lower-thermospheric circulation plays a crucial role in modulating IAV in thermospheric mass density, but additional mechanisms must also contribute to controlling the IAV in $\Sigma O/N_2$. The discrepancy between the simulations and observations warrants further investigation. In addition to achieving a better agreement in the global-mean $\Sigma O/N_2$, the imposed lower-thermospheric circulation also mitigates the well-known thermospheric winter "anomaly" in the TIE-GCM simulation — namely, the positive bias in $\Sigma O/N_2$ between model simulations and observations in the winter hemisphere (e.g., Qian & Yue, 2017) (Figure S3 in the supplement).

The schematic in Figures 4c and d illustrates how the lower-thermospheric circulation couples with the circulation in the thermosphere and thermospheric mass density. Wave forcing from the lower atmosphere drives the lower-thermospheric winter-to-summer circulation, including contributions from tides and GWs. Note that planetary wave (PW) forcing can also modulate the lower-thermospheric circulation during strong PW events (e.g., Yue & Wang, 2014; Gan et al., 2018; Oberheide et al., 2020; Orsolini et al., 2022; Gasperini et al., 2023). The lower-thermospheric circulation is accompanied by upwelling (downwelling) above and downwelling (upwelling) below in the summer (winter) hemisphere to maintain mass continuity. Adiabatic heating and cooling, associated with the additional vertical wind in the nudged run, result in a thermal structure that is warmer (cooler) in the summer (winter) hemisphere below the lower-thermospheric circulation compared to the base run.

The geopotential height is calculated from the hydrostatic equation by vertically integrating the temperature. Changes in the temperature distribution below influence the geopotential height structure above. This dynamical response enhances the latitudinal gradient of geopotential height in the nudged run above the lower-thermospheric circulation. The increased latitudinal gradient of the geopotential height produces a stronger pressure gradient force in the meridional momentum budget above 1.8×10^{-5} hPa. When the nudging terms taper off above the lower-thermospheric circulation in the simulation, which is comparable to the reduction in lower-atmospheric wave forcing above the lower thermosphere, the pressure gradient force efficiently strengthens the summer-to-winter thermospheric circulation between 10^{-5} and 10^{-6} hPa (128 km to 174 km).

Our results demonstrate that the lower-thermospheric circulation modifies the energy budget through adiabatic heating and cooling via changes in vertical wind. Consequently, the thermodynamic balance couples back to the momentum forcing of the pressure gradient, enhancing the summer-to-winter thermospheric circulation. This dynamic and thermodynamic coupling between the lower-thermospheric and thermospheric circulations functions as an atmospheric "gear mechanism". The concept of the "atmospheric gear mechanism" describes how the lower-thermospheric circulation acts as a driver that accelerates the transfer of momentum and energy to higher altitudes by inducing changes in vertical wind. This process resembles a mechanical gear system, where the motion in one layer of the atmosphere amplifies movement in an adjacent layer. This coupling pathway influences the thermospheric dynamics and contributes to the overall redistribution of energy both horizontally and vertically.

The simulated SAO in mass density and $\Sigma O/N_2$ in the nudged run achieves a better agreement with MSIS 2.1, suggesting processes associated with the lower-thermospheric circulation may be an efficient mechanism to modulate the IAV in the coupled ionosphere and thermosphere system (Emmert, 2015; Lean et al., 2016). Because the lower-thermospheric circulation is mainly controlled by the zonal momentum forcing originating from the lower atmospheric waves, this study demonstrates another new lower atmosphere-thermosphere-ionosphere coupling pathway.

5 Discussion

Resolving lower-thermospheric circulation from first principles in thermosphere-ionosphere general circulation models (GCMs) remains challenging due to inadequately resolved, parameterized, or missing wave forcing from the lower atmosphere (Qian & Yue, 2017; Malhotra et al., 2022; J. C. Wang et al., 2022). This limitation may hinder these models' ability to accurately reproduce realistic IAV in the thermosphere and ionosphere (e.g., Qian et al., 2009; Jones et al., 2017; Salinas et al., 2020; Malhotra et al., 2022). The TIE-GCM has a long-standing issue to replicate observed IAV features (Qian et al., 2009). To address this, a seasonally varying K_{zz} has been imposed at the model's lower boundary (e.g., Qian et al., 2009), but this remains an *ad-hoc* approach that compensates for missing mixing and vertical transport processes (Qian et al., 2013; Qian & Yue, 2017). Salinas et al. (2016) further showed that K_{zz} values derived from SABER CO_2 observations exhibit much smaller seasonal variation than in Qian et al. (2009). While this study applies a constant K_{zz} to isolate the impact of the lower-thermospheric circulation, seasonal K_{zz} variations may still influence neutral density and $\Sigma O/N_2$.

Our result suggests including a more realistic lower-thermospheric circulation in the TIE-GCM could reasonably explain the missing physics in the TIE-GCM when considering the mixing and vertical transporting processes that regulate the IAV in thermospheric mass density. Note that, although the lower thermospheric circulation in SD-WACCMX may be underestimated due to the absence of subgrid-scale GW forcing (J. C. Wang et al., 2022), comparing the model results with and without the lower-thermospheric circulation in TIE-GCM still provides valuable insights. This comparison allows for a fundamental understanding of the dynamics that couple the lower-thermospheric circulation with the thermospheric circulation. As demonstrated in Ren et al. (2011) and this study, constraining the horizontal winds and temperature in the lower thermosphere with a more realistic representation may be an solution to improve the IAV in the thermosphere, and in turn, the ionosphere in the GCMs without the lower atmosphere and GW parameterization.

H. Liu et al. (2024) suggested that thermospheric compositional structure can be modulated by circulation changes due to varying GW forcing at higher altitudes, as shown through high- and low-resolution WACCM-X simulations. A similar pathway likely exists to modify thermospheric compositional structure if, as demonstrated in this study, lower-thermospheric circulation modulates thermospheric circulation. This provides an additional plausible explanation for the improved representation of IAV in thermospheric mass density observed in the nudged run, along with the vertical transport of atomic O linked to lower-thermospheric circulation near the base of the thermosphere (e.g., J. C. Wang et al., 2023). Note that, changes in the lower-thermospheric circulation alter background wind and temperature profiles, directly influencing the filtering of GWs that propagate into the thermosphere (Fritts & Alexander, 2003). Meanwhile, dissipating primary GWs can further excite secondary GWs (Vadas et al., 2018). These combined effects should also impact thermospheric circulation and energy distribution and will be further assessed in future studies.

The result in Figure 4a contradicts the conclusion of Jones, Emmert, et al. (2018), who used the NCAR thermosphere-ionosphere-mesosphere-electrodynamics general circulation model (TIME-GCM), an expanded version of TIE-GCM with a lower boundary near 30 km. Jones, Emmert, et al. (2018) proposed that SAO in the IT system arises naturally from variations in interhemispheric atomic oxygen transport via solar-driven thermospheric circulation due to Earth's obliquity. Our findings align with Qian et al. (2009), showing that SAO in thermospheric mass density is absent in TIE-GCM's first principles, even with seasonal variation in solar-driven thermospheric circulation. The lower atmosphere is likely to play a role in influencing the transport of atmospheric mass and, consequently, composition. Addressing this discrepancy is beyond this paper's scope and warrants further investigation.

Our results align with dynamics described by Smith et al. (2019), showing interhemispheric and "upward" coupling from the winter stratosphere to the summer mesosphere through wave-forcing-induced changes in meridional circulation. This process, similar to the atmospheric gear mechanism, leads to global changes in thermal structure through adiabatic heating and cooling associated with changes in vertical wind. Interhemispheric coupling through meridional circulation has been observationally verified by stratospheric ozone and MLT-region CO_2 data (Randel, 1993; N. Wang et al., 2022), providing a solid observational basis supporting the mechanisms proposed herein.

Similarly, sudden stratospheric warmings (SSWs) influence thermosphere-ionosphere dynamics (e.g., Yamazaki et al., 2015; Laskar et al., 2019; Oberheide et al., 2020; Jones et al., 2020; Orsolini et al., 2022), with lower-thermospheric circulation reversals affecting composition and propagating effects into the thermosphere. Jones et al. (2020) showed this variability can impact plasma populations in the topside ionosphere and plasmasphere, with broader implications for inner magnetospheric plasma density.

The "atmospheric gear mechanism" underscores intricate thermospheric coupling, with implications for upper atmospheric science. Incorporating lower-thermospheric circulation in models can improve quiet-time thermospheric conditions and ultimately simulations of geomagnetic storm responses. Similar couplings may exist in other planetary atmospheres but remain poorly understood due to limited observations (e.g., Showman et al., 2010).

Currently, no observational evidence directly links lower-thermospheric circulation to the thermospheric summer-to-winter circulation between 100-300 km. Satellite observations of horizontal winds and O in the mesosphere and thermosphere, with sufficient spatial and temporal coverage, are needed to validate these interactions. While this study focuses on seasonal-scale thermospheric circulation, shorter-term variability may also impact the thermosphere-ionosphere system, as shown numerically by Forbes et al. (2024). The upcoming DYNAMIC and GDC satellite missions will provide critical multi-satellite observations on sub-weekly timescales, helping to resolve these open questions.

6 Closing remarks

In conclusion, our sensitivity study demonstrates that the lower-thermospheric circulation significantly impacts the thermospheric dynamics by modifying the meridional circulation above. The results suggest that adiabatic heating and cooling processes, driven by vertical wind, regulate thermal and momentum structures, strengthening the summer-to-winter circulation in the summer thermosphere and enhancing upwelling at higher latitudes. This circulation coupling further alters the seasonal variation of thermospheric composition. This finding reveals a new coupling mechanism, atmospheric "gear effect", between the lower and upper thermosphere, highlighting the critical role of lower-atmospheric processes in shaping thermospheric behavior. This process functions like a mechanical gear system, where motion in one atmospheric layer amplifies movement in adjacent layers. The interaction of thermal gradients and pressure gradients forms a critical coupling pathway that enhances the upper thermospheric circulation.

From a practical perspective, these findings have implications for improving predictions of thermospheric density, a critical factor for satellite drag estimation and orbital maintenance. The improved representation of IAV in thermospheric mass density provides insights into the previously unresolved discrepancies in TIE-GCM simulations, enabling accurate modeling of thermospheric quiet-time conditions. Such advancements provide a baseline for studying storm-time responses, including the generation of ionospheric irregularities that affect communication and navigation systems.

Since the lower-thermospheric circulation is controlled by wave forcing from the lower atmosphere, this study establishes a new coupling pathway linking the lower atmosphere, thermosphere, and ionosphere through enhanced representation of wave forcing and meridional circulation in the MLT region. This advancement improves the accuracy of models and facilitates better forecasts of space weather events, ultimately aiding satellite operations and mitigating risks posed by thermospheric and ionospheric disturbances. These results underscore the importance of incorporating lower-atmospheric processes into future atmospheric and space weather models.

7 Open Research

TIE-GCM version 3.0 source code can be downloaded from the copy of its Github public repository on Zenodo (NCAR High Altitude Observatory, 2025). SD-WACCMX and the input files are publicly available through a public GitHub repository, `https://github.com/ESCOMP/CESM`. TIE-GCM model output pertinent to this paper can be found via J. C. Wang (2025).

Acknowledgments

This research is supported by NSF Awards AGS-2140031, AGS-2409172, and NASA Goddard Space Flight Center through the Cooperative Agreement 80NSSC21M0180 to Catholic University, Partnership for Heliophysics and Space Environment Research (PHaSER). This work is also supported in part by NASA grants 80NSSC20K1350, 80NSSC20K0189, 80NSSC20K0721, and 80NSSC21K1315, and by NASA DRIVE Science Center for Geospace Storms (CGS) grant 80NSSC22M0163. J.C. Wang acknowledges Dr. Hanli Liu from NCAR/HAO and Dr. Huixin Liu from Kyushu University for their helpful discussions, and Drs. Hao-nan Wu and Dong Lin from NCAR/HAO for their assistance. The National Center for Atmospheric Research is a major facility sponsored by the National Science Foundation under Cooperative Agreement No. 1852977. The scientific color maps (https://doi.org/10.5281/zenodo.1243862; Crameri et al., 2020; Crameri, 2023) are used in figures herein to prevent visual distortion of the data and exclusion of readers with color-vision deficiencies. The authors thank the editor and the reviewers for their careful reading of the manuscript; their comments considerably improved its quality.

References

Andrews, D. G., Leovy, C. B., & Holton, J. R. (1987). *Middle atmosphere dynamics.* Academic press.

Andrews, D. G., & McIntyre, M. E. (1976, November). Planetary Waves in Horizontal and Vertical Shear: The Generalized Eliassen-Palm Relation and the Mean Zonal Acceleration. *Journal of the Atmospheric Sciences*, *33*(11), 2031–2048. Retrieved from `http://journals.ametsoc.org/doi/abs/10.1175/1520-0469%281976%29033%3C2031%3APWIHAV%3E2.0.CO%3B2` (1021 citations (Semantic Scholar/DOI) [2025-01-03] ISBN: 0022492815200469) doi: 10.1175/1520-0469(1976)033<2031:PWIHAV>2.0.CO;2

Bates, D. R. (1959). Some problems concerning the terrestrial atmosphere above about the 100 km level. *Proceedings of the Royal Society of London. Series A. Mathematical and Physical Sciences*, *253*(1275), 451–462. Retrieved from `https://royalsocietypublishing.org/doi/abs/10.1098/rspa.1959.0207` (155 citations (Semantic Scholar/DOI) [2024-11-15] tex.eprint: https://royalsocietypublishing.org/doi/pdf/10.1098/rspa.1959.0207) doi: 10.1098/rspa.1959.0207

Crameri, F. (2023, June). *Scientific colour maps.* Zenodo. Retrieved from `https://doi.org/10.5281/zenodo.8035877` doi: 10.5281/zenodo.8035877

Crameri, F., Shephard, G. E., & Heron, P. J. (2020). The misuse of colour in science communication. *Nature Communications*, *11*(1), 1–10. Retrieved from `http://dx.doi.org/10.1038/s41467-020-19160-7` (11 citations (Semantic Scholar/DOI) [2024-11-15] 21 citations (Semantic Scholar/DOI) [2024-11-15] Publisher: Springer US) doi: 10.1038/s41467-020-19160-7

Dickinson, R. E., Ridley, E. C., & Roble, R. G. (1975). Meridional circulation in the thermosphere i. Equinox conditions. *Journal of Atmospheric Sciences*, *32*(9), 1737 – 1754. Retrieved from `https://journals.ametsoc.org/view/journals/atsc/32/9/1520-0469_1975_032_1737_mcitti_2_0_co_2.xml` (13 citations (Semantic Scholar/DOI) [2024-11-15]) doi: 10.1175/1520-0469(1975)032<1737:MCITTI>2.0.CO;2

Dickinson, R. E., Ridley, E. C., & Roble, R. G. (1977, January). Meridional circulation in the thermosphere. II. Solstice conditions. *Journal of Atmospheric Sciences*, *34*(1), 178–192. (39 citations (Semantic Scholar/DOI) [2024-11-15] 10 citations (Semantic Scholar/DOI) [2024-11-15]) doi: 10.1175/1520-0469(1977)034<0178:MCITTI>2.0.CO;2

Emmert, J. T. (2015). Thermospheric mass density: A review. *Advances in Space Research*, *56*(5), 773–824. Retrieved from `http://dx.doi.org/10.1016/j.asr.2015.05.038` doi: 10.1016/j.asr.2015.05.038

Emmert, J. T., Drob, D. P., Picone, J. M., Siskind, D. E., Jones, M., Mlynczak, M. G., ... Yuan, T. (2021, March). NRLMSIS 2.0: A Whole-Atmosphere Empirical Model of Temperature and Neutral Species Densities. *Earth and Space Science*, *8*(3). Retrieved 2022-08-19, from `https://onlinelibrary.wiley.com/doi/10.1029/2020EA001321` (176 citations (Semantic Scholar/DOI) [2024-11-16]) doi: 10.1029/2020EA001321

Emmert, J. T., Jones, M., Siskind, D. E., Drob, D. P., Picone, J. M., Stevens, M. H., ... Pérot, K. (2022, October). NRLMSIS 2.1: An Empirical Model of Nitric Oxide Incorporated Into MSIS. *Journal of Geophysical Research: Space Physics*, *127*(10). Retrieved 2022-11-23, from `https://onlinelibrary.wiley.com/doi/10.1029/2022JA030896` doi: 10.1029/2022JA030896

Forbes, J. M., Zhang, X., Maute, A., & Cullens, C. (2024, March). Responses of the Mean Thermosphere Circulation, O/N $_2$ Ratio and Ne to Solar and Magnetospheric Forcing From Above and Tidal Forcing From Below. *Journal of Geophysical Research: Space Physics*, *129*(3), e2024JA032449. Retrieved 2024-04-29, from `https://agupubs.onlinelibrary.wiley.com/doi/10.1029/2024JA032449` (37 citations (Semantic Scholar/DOI) [2024-11-15] 179 citations (Semantic Scholar/DOI) [2024-11-15]) doi: 10.1029/2024JA032449

Fritts, D. C., & Alexander, M. J. (2003). Gravity wave dynamics and effects in the middle atmosphere. *Reviews of Geophysics*, *41*(1), 1–64. (2254 citations (Semantic Scholar/DOI) [2025-01-03] ISBN: 8755-1209) doi: 10.1029/2001RG000106

Gan, Q., Oberheide, J., & Pedatella, N. M. (2018, September). Sources, Sinks, and Propagation Characteristics of the Quasi 6-Day Wave and Its Impact on the Residual Mean Circulation. *Journal of Geophysical Research: Atmospheres*, *123*(17), 9152–9170. Retrieved from `http://doi.wiley.com/10.1029/2018JD028553` (32 citations (Semantic Scholar/DOI) [2024-11-16]) doi: 10.1029/2018JD028553

Gan, Q., Qian, L., Pedatella, N. M., & Eastes, R. W. (2024, December). Equinox Transitions of Thermosphere O/N2 and Meridional Circulation in the Northern Hemisphere as Observed by NASA's GOLD and ICON Missions. *Geophysical Research Letters*, *51*(24), e2024GL111810. Retrieved 2025-01-13, from `https://agupubs.onlinelibrary.wiley.com/doi/10.1029/2024GL111810` (0 citations (Semantic Scholar/DOI) [2025-01-13]) doi: 10.1029/2024GL111810

Gan, Q., Qian, L., Pedatella, N. M., Wu, Y., Correira, J., Wang, W., … Eastes, R. W. (2023, February). GOLD Synoptic Observations of Thermospheric Annual and Semiannual Variations in Composition During Solar Minimum Years. *Geophysical Research Letters*, *50*(4). Retrieved 2023-03-23, from `https://onlinelibrary.wiley.com/doi/10.1029/2022GL101215` (254 citations (Semantic Scholar/DOI) [2024-11-15]) doi: 10.1029/2022GL101215

Garcia, R. R. (1989). Dynamics, radiation, and photochemistry in the mesosphere: Implications for the formation of noctilucent clouds. *Journal of Geophysical Research: Atmospheres*, *94*(D12), 14605–14615. Retrieved from `https://agupubs.onlinelibrary.wiley.com/doi/abs/10.1029/JD094iD12p14605` (tex.eprint: https://agupubs.onlinelibrary.wiley.com/doi/pdf/10.1029/JD094iD12p14605) doi: https://doi.org/10.1029/JD094iD12p14605

Gasperini, F., Jr, M. J., Harding, B. J., & Immel, T. J. (2023, April). Direct Observational Evidence of Altered Mesosphere Lower Thermosphere Mean Circulation From a Major Sudden Stratospheric Warming. *Geophysical Re-*

search Letters, *50*(7). (283 citations (Semantic Scholar/DOI) [2024-11-15]) doi: 10.1029/2022GL102579

Hagan, M. E., & Forbes, J. M. (2002). Migrating and nonmigrating diurnal tides in the middle and upper atmosphere excited by tropospheric latent heat release. *Journal of Geophysical Research Atmospheres*, *107*(24), 1–15. (17 citations (Semantic Scholar/DOI) [2024-11-15] ISBN: 0148-0227) doi: 10.1029/2001JD001236

Hagan, M. E., & Forbes, J. M. (2003, February). Migrating and nonmigrating semidiurnal tides in the upper atmosphere excited by tropospheric latent heat release. *Journal of Geophysical Research: Space Physics*, *108*(A2), 4754. Retrieved from http://doi.wiley.com/10.1029/2001JD001236 (21 citations (Semantic Scholar/DOI) [2024-11-15] 27 citations (Semantic Scholar/DOI) [2024-11-15] ISBN: 0148-0227) doi: 10.1029/2002JA009466

Holton, J. R. (1983, October). The Influence of Gravity Wave Breaking on the General Circulation of the Middle Atmosphere. *Journal of the Atmospheric Sciences*, *40*(10), 2497–2507. Retrieved from http://journals.ametsoc.org/doi/10.1175/1520-0469(1983)040%3C2497:TIOGWB%3E2.0.CO;2 (643 citations (Semantic Scholar/DOI) [2024-11-15] ISBN: 9781626239777) doi: 10.1175/1520-0469(1983)040<2497:TIOGWB>2.0.CO;2

Holton, J. R., & Alexander, M. J. (2000). The role of waves in the transport circulation of the middle atmosphere. In *Atmospheric science across the stratopause* (pp. 21–35). American Geophysical Union (AGU). Retrieved from http://doi.wiley.com/10.1029/GM123p0021

Holton, J. R., & Hakim, G. J. (2013). *An Introduction to Dynamic Meteorology.* Elsevier. Retrieved from https://linkinghub.elsevier.com/retrieve/pii/C20090633948 doi: 10.1016/C2009-0-63394-8

Hsu, V. W., Thayer, J. P., Wang, W., & Burns, A. (2016). New insights into the complex interplay between drag forces and its thermospheric consequences. *Journal of Geophysical Research: Space Physics*, *121*(10), 10,417–10,430. (24 citations (Semantic Scholar/DOI) [2025-01-03]) doi: 10.1002/2016JA023058

Jones, M., Drob, D. P., Siskind, D. E., McCormack, J. P., Maute, A., McDonald, S. E., & Dymond, K. F. (2018, December). Evaluating Different Techniques for Constraining Lower Atmospheric Variability in an Upper Atmosphere

General Circulation Model: A Case Study During the 2010 Sudden Stratospheric Warming. *Journal of Advances in Modeling Earth Systems*, *10*(12), 2018MS001440. (22 citations (Semantic Scholar/DOI) [2024-11-15] 30 citations (Semantic Scholar/DOI) [2024-11-15]) doi: 10.1029/2018MS001440

Jones, M., Emmert, J. T., Drob, D. P., Picone, J. M., & Meier, R. R. (2018). Origins of the Thermosphere-Ionosphere Semiannual Oscillation: Reformulating the "Thermospheric Spoon" Mechanism. *Journal of Geophysical Research: Space Physics*, *123*(1), 931–954. (33 citations (Semantic Scholar/DOI) [2025-01-03]) doi: 10.1002/2017JA024861

Jones, M., Emmert, J. T., Drob, D. P., & Siskind, D. E. (2017). Middle atmosphere dynamical sources of the semiannual oscillation in the thermosphere and ionosphere. *Geophysical Research Letters*, *44*(1), 12–21. (1 citations (Semantic Scholar/DOI) [2024-11-15] 11 citations (Semantic Scholar/DOI) [2024-11-15] 31 citations (Semantic Scholar/DOI) [2024-11-15]) doi: 10.1002/2016GL071741

Jones, M., Siskind, D. E., Drob, D. P., McCormack, J. P., Emmert, J. T., Dhadly, M. S., … Jacobi, C. (2020, October). Coupling From the Middle Atmosphere to the Exobase: Dynamical Disturbance Effects on Light Chemical Species. *Journal of Geophysical Research: Space Physics*, *125*(10). Retrieved 2022-11-28, from `https://onlinelibrary.wiley.com/doi/10.1029/2020JA028331` (31 citations (Semantic Scholar/DOI) [2024-11-15]) doi: 10.1029/2020JA028331

Laskar, F. I., McCormack, J. P., Chau, J. L., Pallamraju, D., Hoffmann, P., & Singh, R. P. (2019). Interhemispheric Meridional Circulation During Sudden Stratospheric Warming. *Journal of Geophysical Research: Space Physics*, *124*(8), 7112–7122. (26 citations (Semantic Scholar/DOI) [2025-01-03]) doi: 10.1029/2018JA026424

Lean, J. L., Meier, R. R., Picone, J. M., Sassi, F., Emmert, J. T., & Richards, P. G. (2016, October). Ionospheric total electron content: Spatial patterns of variability. *Journal of Geophysical Research: Space Physics*, *121*(10). Retrieved 2024-04-29, from `https://agupubs.onlinelibrary.wiley.com/doi/10.1002/2016JA023210` (42 citations (Semantic Scholar/DOI) [2025-01-03]) doi: 10.1002/2016JA023210

Liu, H., Lauritzen, P. H., & Vitt, F. (2024, February). Impacts of Gravity

Waves on the Thermospheric Circulation and Composition. *Geophysical Research Letters*, *51*(3), e2023GL107453. Retrieved 2024-02-09, from https://agupubs.onlinelibrary.wiley.com/doi/10.1029/2023GL107453 doi: 10.1029/2023GL107453

Liu, H.-L., Bardeen, C. G., Foster, B. T., Lauritzen, P., Liu, J., Lu, G., … Wang, W. (2018, February). Development and Validation of the Whole Atmosphere Community Climate Model With Thermosphere and Ionosphere Extension (WACCM-X 2.0). *Journal of Advances in Modeling Earth Systems*, *10*(2), 381–402. Retrieved from http://doi.wiley.com/10.1002/2017MS001232 (252 citations (Semantic Scholar/DOI) [2024-11-15]) doi: 10.1002/2017MS001232

Liu, J., Liu, H., Wang, W., Burns, A. G., Wu, Q., Gan, Q., … Schreiner, W. S. (2018, February). First Results From the Ionospheric Extension of WACCM-X During the Deep Solar Minimum Year of 2008. *Journal of Geophysical Research: Space Physics*, *123*(2), 1534–1553. Retrieved 2022-08-11, from https://onlinelibrary.wiley.com/doi/10.1002/2017JA025010 (55 citations (Semantic Scholar/DOI) [2025-01-03]) doi: 10.1002/2017JA025010

Malhotra, G., Ridley, A. J., & Jones, M. (2022, February). Impacts of Lower Thermospheric Atomic Oxygen and Dynamics on the Thermospheric Semiannual Oscillation Using GITM and WACCM-X. *Journal of Geophysical Research: Space Physics*, *127*(2). Retrieved 2022-04-01, from https://onlinelibrary.wiley.com/doi/10.1029/2021JA029320 (2 citations (Semantic Scholar/DOI) [2025-01-03]) doi: 10.1029/2021JA029320

Maute, A., Hagan, M. E., Yudin, V., Liu, H., & Yizengaw, E. (2015, June). Causes of the longitudinal differences in the equatorial vertical E×B drift during the 2013 SSW period as simulated by the TIME-GCM. *Journal of Geophysical Research: Space Physics*, *120*(6), 5117–5136. Retrieved 2021-10-14, from https://onlinelibrary.wiley.com/doi/abs/10.1002/2015JA021126 (27 citations (Semantic Scholar/DOI) [2024-11-15]) doi: 10.1002/2015JA021126

Mlynczak, M., Yue, J., McCormack, J., Liebermann, R., & Livesey, N. (2021, March). An Observational Gap at the Edge of Space. *Eos*, *102*. Retrieved 2024-10-03, from https://eos.org/opinions/an-observational-gap-at-the-edge-of-space (9 citations (Semantic Scholar/DOI) [2024-11-15]) doi:

10.1029/2021EO155494

NCAR High Altitude Observatory. (2025, April). *TIEGCM v3.0.* Zenodo. doi: 10.5281/zenodo.15214471

Oberheide, J., Pedatella, N. M., Gan, Q., Kumari, K., Burns, A. G., & Eastes, R. W. (2020). Thermospheric Composition O/N 2 Response to an Altered Meridional Mean Circulation During Sudden Stratospheric Warmings Observed by GOLD. *Geophysical Research Letters*, *47*(1), 1–7. (49 citations (Semantic Scholar/DOI) [2024-11-15] 38 citations (Semantic Scholar/DOI) [2024-11-15]) doi: 10.1029/2019GL086313

Orsolini, Y. J., Zhang, J., & Limpasuvan, V. (2022, October). Abrupt Change in the Lower Thermospheric Mean Meridional Circulation During Sudden Stratospheric Warmings and Its Impact on Trace Species. *Journal of Geophysical Research: Atmospheres*, *127*(20). Retrieved 2023-01-24, from `https://onlinelibrary.wiley.com/doi/10.1029/2022JD037050` (80 citations (Semantic Scholar/DOI) [2024-11-15]) doi: 10.1029/2022JD037050

Qian, L., Burns, A. G., Solomon, S. C., & Wang, W. (2013, May). Annual/semiannual variation of the ionosphere. *Geophysical Research Letters*, *40*(10), 1928–1933. Retrieved 2024-04-29, from `https://agupubs.onlinelibrary.wiley.com/doi/10.1002/grl.50448` (21 citations (Semantic Scholar/DOI) [2024-11-15]) doi: 10.1002/grl.50448

Qian, L., Solomon, S. C., & Kane, T. J. (2009). Seasonal variation of thermospheric density and composition. *Journal of Geophysical Research: Space Physics*, *114*(1), 1–15. (4 citations (Semantic Scholar/DOI) [2024-11-15] ISBN: 978-84-942134-8-9) doi: 10.1029/2008JA013643

Qian, L., & Yue, J. (2017). Impact of the lower thermospheric winter-to-summer residual circulation on thermospheric composition. *Geophysical Research Letters*, *44*(9), 3971–3979. (28 citations (Semantic Scholar/DOI) [2025-01-03]) doi: 10.1002/2017GL073361

Randel, W. J. (1993). Global variations of zonal mean ozone during stratospheric warming events. *Journal of Atmospheric Sciences*, *50*(19), 3308 – 3321. Retrieved from `https://journals.ametsoc.org/view/journals/atsc/50/19/1520-0469_1993_050_3308_gvozmo_2_0_co_2.xml` (11 citations (Semantic Scholar/DOI) [2024-11-15] 14 citations (Semantic Scholar/DOI) [2024-11-15]

Place: Boston MA, USA Publisher: American Meteorological Society) doi: 10.1175/1520-0469(1993)050<3308:GVOZMO>2.0.CO;2

Ren, S., Polavarapu, S., Beagley, S. R., Nezlin, Y., & Rochon, Y. J. (2011). The impact of gravity wave drag on mesospheric analyses of the 2006 stratospheric major warming. *Journal of Geophysical Research Atmospheres*, *116*(19), 1–18. (22 citations (Semantic Scholar/DOI) [2024-11-15]) doi: 10.1029/2011JD015943

Roble, R. G., Ridley, E. C., & Dickinson, R. E. (1987). On the global mean structure of the thermosphere. *Journal of Geophysical Research*, *92*(A8), 8745. Retrieved 2022-11-05, from `http://doi.wiley.com/10.1029/JA092iA08p08745` (278 citations (Semantic Scholar/DOI) [2024-11-16]) doi: 10.1029/JA092iA08p08745

Salinas, C. C. J. H., Chang, L. C., Liang, M., Yue, J., Qian, L., Gan, Q., ... Mlynczak, M. (2020, March). Local-Time Variabilities of March Equinox Daytime SABER CO $_2$ in the Upper Mesosphere and Lower Thermosphere Region. *Journal of Geophysical Research: Space Physics*, *125*(3). Retrieved 2022-04-16, from `https://onlinelibrary.wiley.com/doi/abs/10.1029/2019JA027039` (27 citations (Semantic Scholar/DOI) [2024-11-15]) doi: 10.1029/2019JA027039

Salinas, C. C. J. H., Chang, L. C., Liang, M.-C., Yue, J., Russell, J., & Mlynczak, M. (2016, December). Impacts of SABER CO 2 -based eddy diffusion coefficients in the lower thermosphere on the ionosphere/thermosphere. *Journal of Geophysical Research: Space Physics*, *121*(12), 12,080–12,092. Retrieved from `http://doi.wiley.com/10.1002/2016JA023161` (18 citations (Semantic Scholar/DOI) [2024-11-15] 43 citations (Semantic Scholar/DOI) [2024-11-15] ISBN: 2169-9402) doi: 10.1002/2016JA023161

Showman, A. P., Cho, J. Y. K., & Menou, K. (2010). Atmospheric circulation of exoplanets. In S. Seager (Ed.), *Exoplanets* (pp. 471–516). (tex.adsnote: Provided by the SAO/NASA Astrophysics Data System) doi: 10.48550/arXiv.0911.3170

Siskind, D. E., & Drob, D. P. (2014). Use of NOGAPS-ALPHA as a Bottom Boundary for the NCAR/TIEGCM. *Modeling the Ionosphere-Thermosphere System*, *9780875904*, 171–180. (9 citations (Semantic Scholar/DOI) [2025-01-03] ISBN:

9781118704417) doi: 10.1002/9781118704417.ch15

Siskind, D. E., Drob, D. P., Dymond, K. F., & McCormack, J. P. (2014, February). Simulations of the effects of vertical transport on the thermosphere and ionosphere using two coupled models. *Journal of Geophysical Research: Space Physics*, *119*(2), 1172–1185. Retrieved from `http://doi.wiley.com/10.1002/2013JA019116` (41 citations (Semantic Scholar/DOI) [2025-01-03] ISBN: 9780273725596) doi: 10.1002/2013JA019116

Smith, A. K., Pedatella, N. M., & Mullen, Z. K. (2019, March). Interhemispheric Coupling Mechanisms in the Middle Atmosphere of WACCM6. *Journal of the Atmospheric Sciences*, *77*(3), 1101–1118. Retrieved from `https://journals.ametsoc.org/jas/article/77/3/1101/345896/Interhemispheric-Coupling-Mechanisms-in-the-Middle` (25 citations (Semantic Scholar/DOI) [2024-11-15]) doi: 10.1175/JAS-D-19-0253.1

Strickland, D. J., Meier, R. R., Walterscheid, R. L., Craven, J. D., Christensen, A. B., Paxton, L. J., ... Crowley, G. (2004, January). Quiet-time seasonal behavior of the thermosphere seen in the far ultraviolet dayglow. *Journal of Geophysical Research: Space Physics*, *109*(A1), 2003JA010220. Retrieved 2025-01-27, from `https://agupubs.onlinelibrary.wiley.com/doi/10.1029/2003JA010220` (102 citations (Semantic Scholar/DOI) [2025-01-27]) doi: 10.1029/2003JA010220

Vadas, S. L., Zhao, J., Chu, X., & Becker, E. (2018, September). The Excitation of Secondary Gravity Waves From Local Body Forces: Theory and Observation. *Journal of Geophysical Research: Atmospheres*, *123*(17), 9296–9325. Retrieved 2022-07-31, from `http://doi.wiley.com/10.1029/2017JD027970` (107 citations (Semantic Scholar/DOI) [2025-01-03]) doi: 10.1029/2017JD027970

Wang, J. C. (2025, April). *Dataset for "modulation of thermospheric circulation by lower-thermospheric winter-to- summer circulation: The atmospheric gear effect" (wang et al., 2025).* Zenodo. Retrieved from `https://doi.org/10.5281/zenodo.15205002` doi: 10.5281/zenodo.15205002

Wang, J. C., Chang, L. C., Yue, J., Wang, W., & Siskind, D. E. (2017, May). The quasi 2 day wave response in TIME-GCM nudged with NOGAPS-ALPHA. *Journal of Geophysical Research: Space Physics*, *122*(5), 5709–5732. Retrieved from `http://doi.wiley.com/10.1002/2016JA023745` (23 citations (Semantic

Scholar/DOI) [2024-11-16]) doi: 10.1002/2016JA023745

Wang, J. C., Yue, J., Wang, W., Qian, L., Jones, M., & Wang, N. (2023, November). The Lower Thermospheric Winter-To-Summer Meridional Circulation: 2. Impact on Atomic Oxygen. *Journal of Geophysical Research: Space Physics*, *128*(11), e2023JA031684. Retrieved 2023-11-05, from `https://agupubs.onlinelibrary.wiley.com/doi/10.1029/2023JA031684` (0 citations (Semantic Scholar/DOI) [2024-11-16]) doi: 10.1029/2023JA031684

Wang, J. C., Yue, J., Wang, W., Qian, L., Wu, Q., & Wang, N. (2022, December). The Lower Thermospheric Winter-To-Summer Meridional Circulation: 1. Driving Mechanism. *Journal of Geophysical Research: Space Physics*, *127*(12). Retrieved 2022-12-01, from `https://onlinelibrary.wiley.com/doi/10.1029/2022JA030948` (22 citations (Semantic Scholar/DOI) [2024-11-15]) doi: 10.1029/2022JA030948

Wang, N., Qian, L., Yue, J., Wang, W., Mlynczak, M. G., & Russell, J. M. (2022, February). Climatology of Mesosphere and Lower Thermosphere Residual Circulations and Mesopause Height Derived From SABER Observations. *Journal of Geophysical Research: Atmospheres*, *127*(4). Retrieved 2022-02-25, from `https://onlinelibrary.wiley.com/doi/10.1029/2021JD035666` (10 citations (Semantic Scholar/DOI) [2024-11-16]) doi: 10.1029/2021JD035666

Xu, J., Liu, H., Yuan, W., Smith, A. K., Roble, R. G., Mertens, C. J., … Mlynczak, M. G. (2007, May). Mesopause structure from Thermosphere, Ionosphere, Mesosphere, Energetics, and Dynamics (TIMED)/Sounding of the Atmosphere Using Broadband Emission Radiometry (SABER) observations. *Journal of Geophysical Research: Atmospheres*, *112*(D9), 2006JD007711. Retrieved 2024-10-03, from `https://agupubs.onlinelibrary.wiley.com/doi/10.1029/2006JD007711` (95 citations (Semantic Scholar/DOI) [2025-01-03]) doi: 10.1029/2006JD007711

Yamazaki, Y., Kosch, M. J., & Emmert, J. T. (2015). Evidence for stratospheric sudden warming effects on the upper thermosphere derived from satellite orbital decay data during 1967-2013. *Geophysical Research Letters*, *42*(15), 6180–6188. (28 citations (Semantic Scholar/DOI) [2025-01-03]) doi: 10.1002/2015GL065395

Yamazaki, Y., & Richmond, A. D. (2013, September). A theory of ionospheric response to upward-propagating tides: Electrodynamic effects and tidal mixing effects. *Journal of Geophysical Research: Space Physics*, *118*(9), 5891–5905. Retrieved 2014-11-13, from http://doi.wiley.com/10.1002/jgra.50487 (85 citations (Semantic Scholar/DOI) [2024-11-15]) doi: 10.1002/jgra.50487

Yue, J., Jian, Y., Wang, W., Meier, R., Burns, A., Qian, L., . . . Mlynczak, M. (2019, April). Annual and Semiannual Oscillations of Thermospheric Composition in TIMED/GUVI Limb Measurements. *Journal of Geophysical Research: Space Physics*, 2019JA026544. Retrieved 2022-01-11, from https://onlinelibrary.wiley.com/doi/abs/10.1029/2019JA026544 (125 citations (Semantic Scholar/DOI) [2024-11-15] 40 citations (Semantic Scholar/DOI) [2024-11-15]) doi: 10.1029/2019JA026544

Yue, J., & Wang, N. (2025, April). Estimation of adiabatic cooling and warming in the mesosphere and lower thermosphere. *Journal of Atmospheric and Solar-Terrestrial Physics*, *269*, 106492. Retrieved 2025-04-12, from https://linkinghub.elsevier.com/retrieve/pii/S1364682625000768 doi: 10.1016/j.jastp.2025.106492

Yue, J., & Wang, W. (2014, March). Changes of thermospheric composition and ionospheric density caused by quasi 2 day wave dissipation. *Journal of Geophysical Research: Space Physics*, *119*(3), 2069–2078. Retrieved from http://doi.wiley.com/10.1002/2013JA019725 (41 citations (Semantic Scholar/DOI) [2024-11-15]) doi: 10.1002/2013JA019725